Journal of Solid State Chemistry **149,** 92–98 (2000)
Article ID jssc.1999.8502, available online at http://www.idealibrary.com on IDEAL®

Negative Thermal Expansion in $Y_2(WO_4)_3$

David A. Woodcock,* Philip Lightfoot,*,[1] and Clemens Ritter†

* *School of Chemistry, University of St. Andrews, North Haugh, St. Andrews, Fife, Scotland KY16 9ST; and*
† *Institut Laue Langevin, BP 156, 38042, Grenoble Cedex 9, France*

Received April 15, 1999; in revised form May 28, 1999; accepted September 15, 1999

We present the results of neutron powder diffraction experiments with the D2B instrument at Institut Laue Langevin on $Al_2(WO_4)_3$ and $Y_2(WO_4)_3$ over the temperature range 20 to 800°C. The coefficients of thermal expansion are determined to be $\alpha_a = -1.31 \times 10^{-6}\,°C^{-1}$, $\alpha_b = 5.94 \times 10^{-6}\,°C^{-1}$, and $\alpha_c = -9.94 \times 10^{-6}\,°C^{-1}$ for $Al_2(WO_4)_3$ and $\alpha_a = -10.35 \times 10^{-6}\,°C^{-1}$, $\alpha_b = -3.06 \times 10^{-6}\,°C^{-1}$, and $\alpha_c = -7.62 \times 10^{-6}\,°C^{-1}$ for $Y_2(WO_4)_3$. As in the case of $Lu_2(WO_4)_3$, the expansivity is unusual in the case of $Y_2(WO_4)_3$, as the negative thermal expansion is present along all three axes.

INTRODUCTION

The field of negative thermal expansion materials is broadening considerably at the moment, with attention being focused on both microporous materials, such as ITQ-1 (1) and AlPO-17 (2), and materials with the general formula $A_2M_3O_{12}$, such as $NaTi_2(PO_4)_3$ (3, 4) and $Sc_2(WO_4)_3$ (5). $Sc_2(WO_4)_3$ has been known to exhibit these properties for some time: its axial contraction was reported by Balashov *et al.* (6) with $\alpha_a = -5.83$, $\alpha_b = +4.03$, $\alpha_c = -1.91$, and $\alpha_V = -3.64 \times 10^{-6}\,°C^{-1}$. However, it is only recently that the technique of neutron powder diffraction has been employed to elucidate the mechanism and factors governing the magnitude of expansivity within this system.

The scandium tungstate structure consists of a corner-sharing network of ScO_6 octahedra and WO_4 tetrahedra crystallizing in space group *Pnca*. The ScO_6 octahedron shares corners with six WO_4 tetrahedra and the WO_4 tetrahedron shares corners with four ScO_6 octahedra. There are two crystallographically distinct W sites, one (W1) on a twofold axis and the other on a general position (8*d*). A polyhedral representation of this structure is shown in Fig. 1.

It has been suggested by Forster *et al.* (7) that the magnitude of thermal expansivity within the system is related to the size of the *A* cation. Larger *A* cations are suggested to lead to more negative coefficients of thermal expansion. Previous to this work $Lu_2(WO_4)_3$ (7) was the material with the largest cation to have been studied. The linear thermal expansion coefficient was found to be $-6.8 \times 10^{-6}\,°C^{-1}$, the strongest thermal contraction to be found for this structure type. However, the upper tolerance limit for the $Sc_2(WO_4)_3$ structure is $Y_2(WO_4)_3$, the Y^{3+} cation having an ionic radius of 1.01 Å, compared with 0.98 Å for Lu^{3+}. In this paper, the behavior of this material is contrasted with that of $Al_2(WO_4)_3$, the Al^{3+} radius being 0.535 Å. These materials represent the extremes of size compatibility of the *A* cation within this structure type, and should therefore reveal extremes of behavior. $Al_2(WO_4)_3$ has been previously studied by Evans *et al.* (8) using both dilatometer and X-ray powder diffraction data, which revealed bulk thermal expansivities of -3 and $+2.2 \times 10^{-6}\,°C^{-1}$, respectively. The intermediate phase $YAl(WO_4)_3$ was also reported as having an α of $5 \times 10^{-6}\,°C^{-1}$, based on dilatometer data. Axial thermal expansion coefficients, determined from diffraction data, were not reported for either $Al_2(WO_4)_3$ or $YAl(WO_4)_3$.

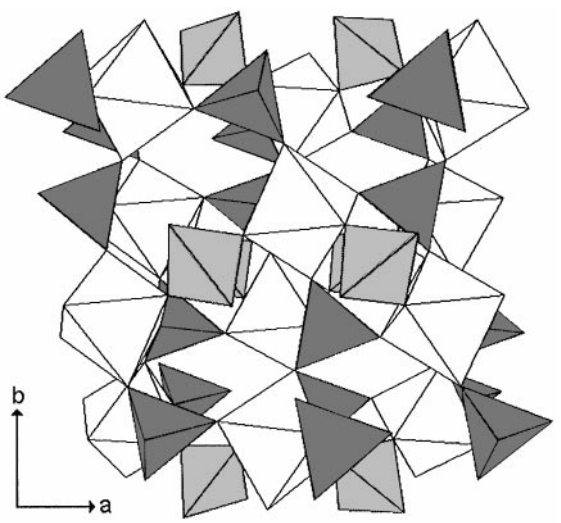

FIG. 1. Structure of $Y_2(WO_4)_3$ showing YO_6 octahedra (white), $W(1)O_4$ tetrahedra (light gray), and $W(2)O_4$ tetrahedra (dark gray).

[1]To whom correspondence should be addressed. E-mail: pl@st-and.ac.uk.

0022-4596/00 $35.00

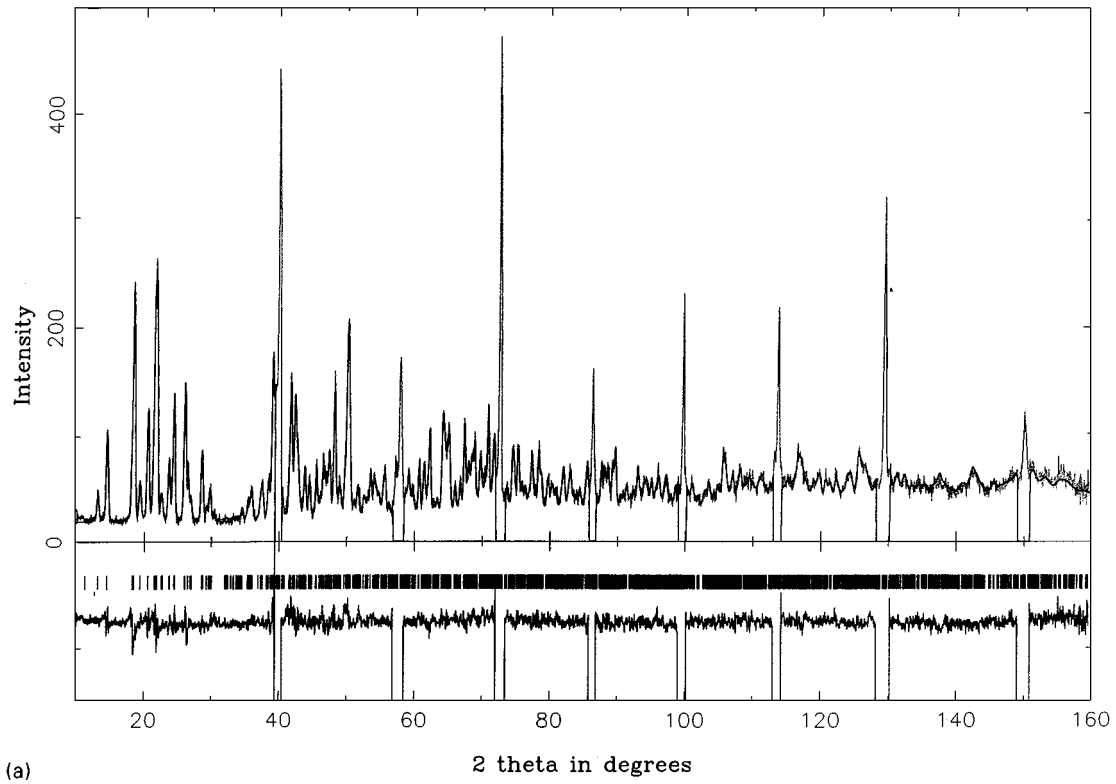

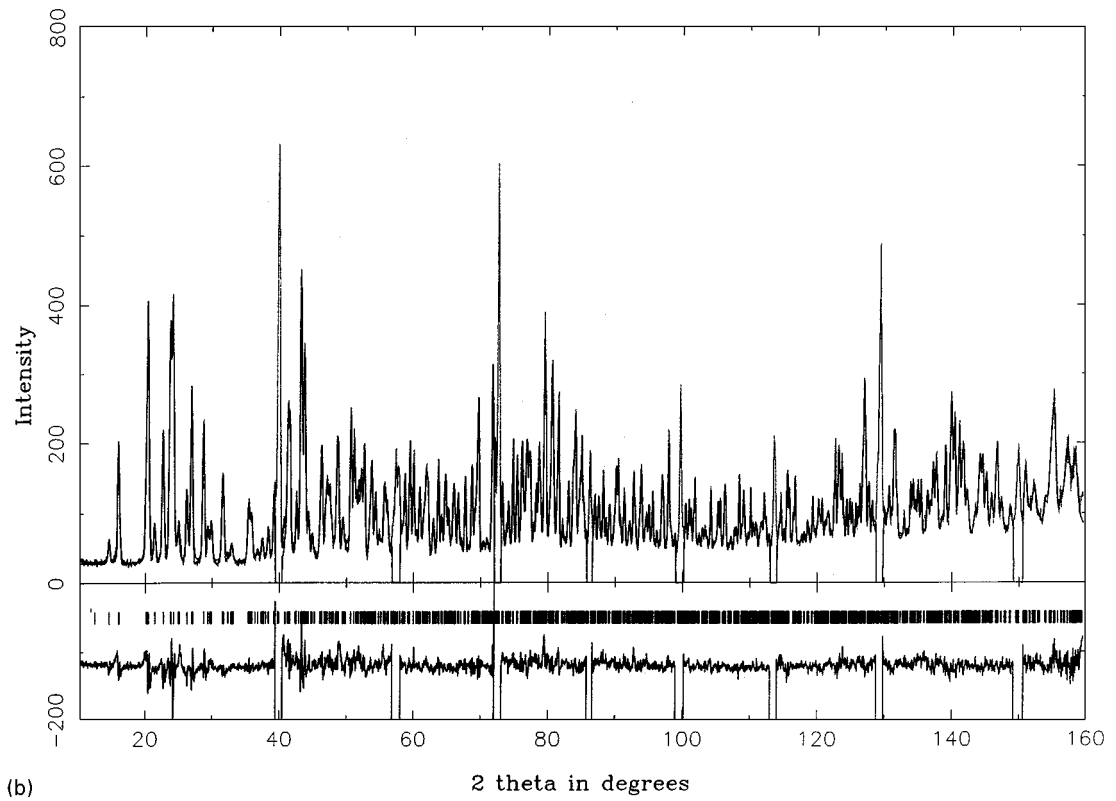

FIG. 2. Typical neutron Rietveld plots for (a) $Y_2(WO_4)_3$ and (b) $Al_2(WO_4)_3$. The excluded regions are due to Nb peaks from the furnace.

EXPERIMENTAL

Samples were prepared using the starting materials Al_2O_3 (99.99%, Aldrich), WO_3 (99+%, Aldrich), and Y_2O_3 (99.99%, Aldrich). $Al_2(WO_4)_3$ was synthesized using a heat treatment of 24 h at 1000°C in a Pt crucible, the starting

TABLE 1
Atom Positions for $Y_2(WO_4)_3$ and $Al_2(WO_4)_3$ at 20 and 800°C

$Al_2(WO_4)_3$ 20°C
$R_p = 6.55$, $R_{wp} = 8.88$, $\chi^2 = 3.09$
Space group *Pnca*
$a = 9.1364(2)$ Å, $b = 12.5913(3)$ Å, $c = 9.0560(2)$ Å

	x	*y*	*z*	*B*[a]	Multiplicity
Al	0.4668(8)	0.3798(7)	0.2498(9)	0.6(1)	8*d*
W1	0.25	0	0.4750(8)	0.3(2)	4*c*
W2	0.1166(5)	0.3571(4)	0.3948(5)	0.3(2)	8*d*
O1	0.0900(4)	0.1405(4)	0.0878(5)	1.1(2)	8*d*
O2	0.1223(6)	0.0671(4)	0.3645(5)	1.3(2)	8*d*
O3	0.0055(4)	0.2572(4)	0.3172(6)	1.2(2)	8*d*
O4	0.3381(6)	0.4050(4)	0.0885(6)	1.1(2)	8*d*
O5	0.0697(5)	0.4791(4)	0.3210(6)	1.2(2)	8*d*
O6	0.3057(5)	0.3308(4)	0.3608(6)	1.2(2)	8*d*

$Al_2(WO_4)_3$ 800°C
$R_p = 6.96$, $R_{wp} = 9.56$, $\chi^2 = 3.72$
Space group *Pnca*
$a = 9.1267(4)$ Å, $b = 12.6488(6)$ Å, $c = 9.0546(4)$ Å

	x	*y*	*z*	*B*[a]	Multiplicity
Al	0.471(1)	0.382(1)	0.246(2)	1.9(2)	8*d*
W1	0.25	0	0.471(2)	1.4(2)	4*c*
W2	0.113(1)	0.355(1)	0.392(1)	1.4(2)	8*d*
O1	0.091(1)	0.138(1)	0.085(1)	3.8(3)	8*d*
O2	0.132(1)	0.070(1)	0.360(1)	4.8(3)	8*d*
O3	0.006(1)	0.257(1)	0.316(1)	3.5(2)	8*d*
O4	0.343(1)	0.410(1)	0.084(1)	3.1(2)	8*d*
O5	0.065(1)	0.480(1)	0.319(1)	3.8(3)	8*d*
O6	0.307(1)	0.336(1)	0.356(1)	3.4(2)	8*d*

$Y_2(WO_4)_3$ 20°C
$R_p = 7.34$, $R_{wp} = 9.26$, $\chi^2 = 1.77$
Space group *Pnca*
$a = 10.070(1)$ Å, $b = 13.937(1)$ Å, $c = 9.980(1)$ Å

	x	*y*	*z*	*B*	Multiplicity
Y	0.470(1)	0.381(1)	0.250(1)	0.9(1)	8*d*
W1	0.25	0	0.475(1)	0.4(2)	4*c*
W2	0.113(1)	0.357(1)	0.392(1)	0.8(2)	8*d*
O1	0.089(1)	0.141(1)	0.066(1)	1.8(2)	8*d*
O2	0.139(1)	0.065(1)	0.371(1)	1.8(2)	8*d*
O3	0.016(1)	0.265(1)	0.319(1)	2.1(2)	8*d*
O4	0.339(1)	0.416(1)	0.075(1)	2.5(2)	8*d*
O5	0.066(1)	0.468(1)	0.324(1)	2.1(2)	8*d*
O6	0.284(1)	0.337(1)	0.356(1)	2.2(2)	8*d*

TABLE 1—*Continued*

$Y_2(WO_4)_3$ 800°C
$R_p = 7.57$, $R_{wp} = 9.65$, $\chi^2 = 1.98$
Space group *Pnca*
$a = 9.986(2)$ Å, $b = 13.905(2)$ Å, $c = 9.919(2)$ Å

	x	*y*	*z*	*B*	Multiplicity
Y	0.472(1)	0.384(1)	0.248(2)	1.7(1)	8*d*
W1	0.25	0	0.481(3)	1.9(2)	4*c*
W2	0.111(3)	0.358(2)	0.390(2)	2.4(2)	8*d*
O1	0.089(2)	0.140(2)	0.066(2)	2.4(2)	8*d*
O2	0.144(3)	0.066(2)	0.361(3)	4.7(2)	8*d*
O3	0.021(2)	0.266(2)	0.320(3)	5.1(2)	8*d*
O4	0.341(3)	0.421(2)	0.081(3)	5.7(2)	8*d*
O5	0.063(2)	0.462(2)	0.326(3)	4.5(2)	8*d*
O6	0.286(2)	0.342(2)	0.360(2)	3.7(2)	8*d*

[a] Equivalent isotropic temperature factor.

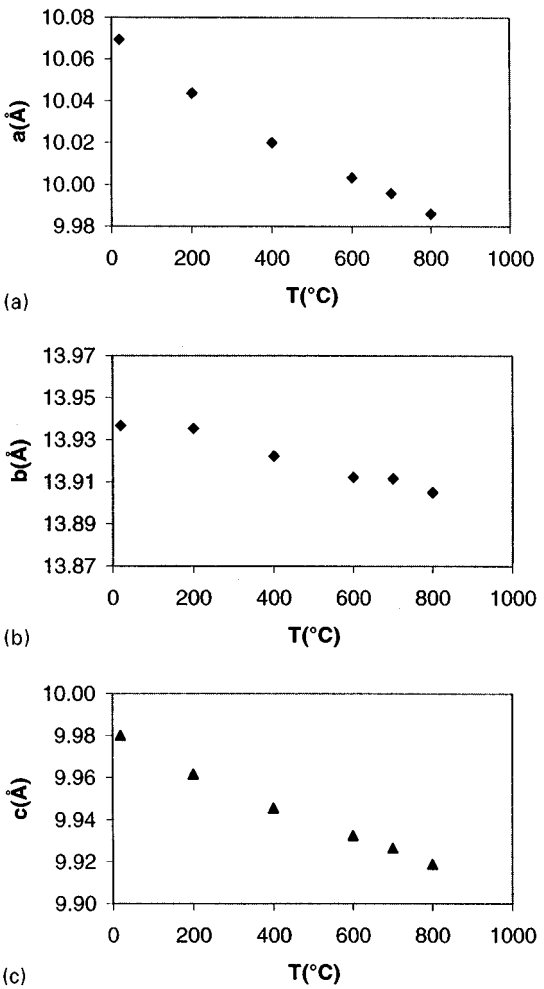

FIG. 3. Plots of the evolution of unit cell parameters versus temperature for $Y_2(WO_4)_3$ for the (a) *a* axis, (b) *b* axis, and (c) *c* axis.

materials being intimately ground under acetone. For $Y_2(WO_4)_3$ the treatment consisted of 24 h at 900°C, followed by 24 h at 1000°C and 24 h at 1100°C. The samples were characterized on a Philips PW3710 diffractometer using Cu$K\alpha$ radiation. This revealed the samples to be phase pure.

The neutron diffraction experiment was carried out on the D2B instrument at the Institut Laue Langevin, Grenoble, France, over the temperature range 20–800°C at a wavelength of 1.596 Å. Data were collected for approximately 3.5 h at each temperature. Data were refined using the FULLPROF (9) program, atom positions from Abraham and Bernstein's solution of the $Sc_2(WO_4)_3$ structure (10) in space group *Pnca*, and a pseudo-Voigt profile function. Typical neutron Rietveld plots for $Y_2(WO_4)_3$ and $Al_2(WO_4)_3$ are shown in Fig. 2 and the resulting atomic coordinates in Table 1. The errors are much smaller in the $Al_2(WO_4)_3$ sample than in the $Y_2(WO_4)_3$ sample as the data are much better resolved at high angles. For this reason, we have carried out a full anisotropic refinement of all atoms in $Al_2(WO_4)_3$ but only an isotropic refinement for $Y_2(WO_4)_3$.

RESULTS AND DISCUSSION

Plots of the evolution of unit cell parameters and cell volume against temperature are shown in Figs. 3–6. $Y_2(WO_4)_3$ shows negative thermal expansion along all three axes; the coefficients of thermal expansion are shown in Table 2. This leads to an overall volume contraction of $-20.9\times10^{-6\circ}C^{-1}$. $Al_2(WO_4)_3$ shows a slight contraction along both the *a* and *c* axes, but the strong expansion of the *b* axis leads to an overall volume expansion of $4.51\times10^{-6\circ}C^{-1}$. As expected $Y_2(WO_4)_3$ shows a negative thermal expansion similar to, but slightly more enhanced than, that of $Lu_2(WO_4)_3$, and both the latter show behavior dramatically different from that of $Al_2(WO_4)_3$ and $Sc_2(WO_4)_3$. Behavior is correlated with ionic size.

Evans *et al.* (5) carried out an elegant and detailed analysis of the thermal expansion behavior of $Sc_2(WO_4)_3$. Their modeling of the structure using an isotropic free atom scheme suggested that the WO_4 and ScO_6 polyhedra could be regarded as rigid. They therefore imposed such a

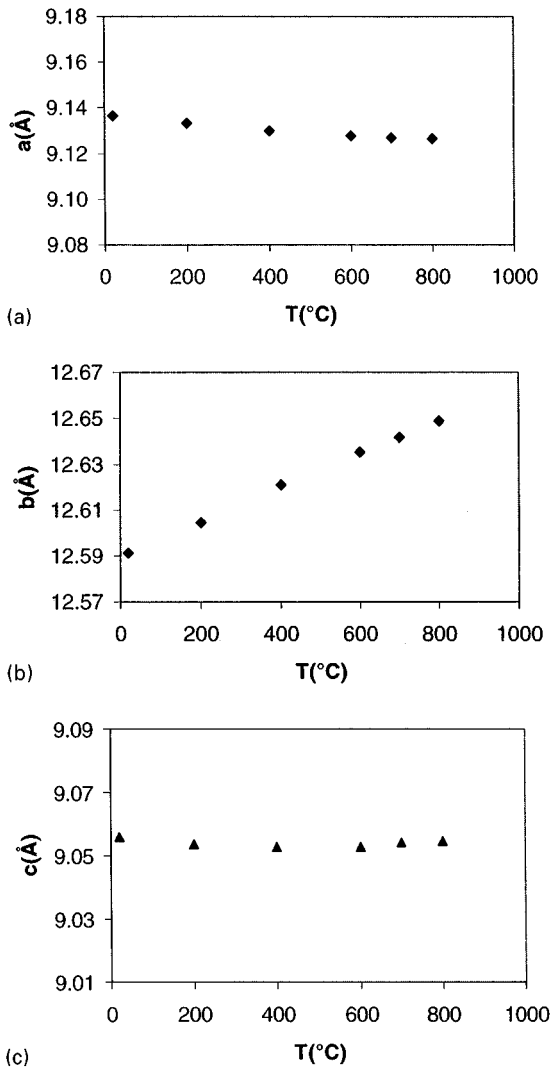

FIG. 5. Plots of the evolution of unit cell parameters versus temperature for $Al_2(WO_4)_3$ for the (a) *a* axis, (b) *b* axis, and (c) *c* axis.

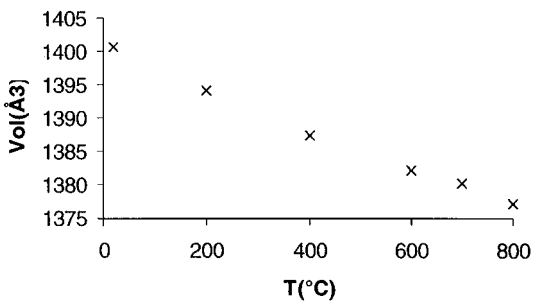

FIG. 4. Plot of the evolution of unit cell volume versus temperature for $Y_2(WO_4)_3$.

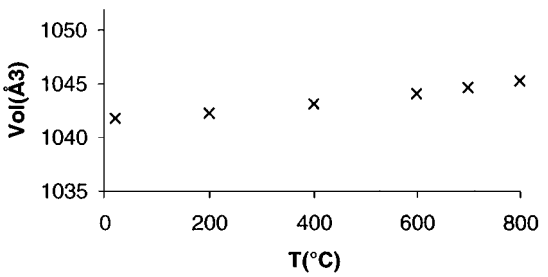

FIG. 6. Plot of the evolution of unit cell volume versus temperature for $Al_2(WO_4)_3$.

TABLE 2
Coefficients of Thermal Expansion for $M_2(WO_4)_3$ Materials

Sample	Ionic radius for M^{3+} (Å)	α_a ($\times 10^{-6}$ °C^{-1})	α_b ($\times 10^{-6}$ °C^{-1})	α_c ($\times 10^{-6}$ °C^{-1})	V ($\times 10^{-6}$ °C^{-1})	Ref.
$Al_2(WO_4)_3$	0.535	− 1.31	5.94	− 0.099	4.51	This work
$Sc_2(WO_4)_3$	0.745	− 6.3	7.5	− 5.5	− 6.5	5
$Lu_2(WO_4)_3$	0.98	− 9.9	− 2.2	− 8.3	− 20.4	7
$Y_2(WO_4)_3$	1.01	− 10.35	− 3.06	− 7.62	− 20.9	This work

constraint on their model, reducing the complexity of the refinement and producing better fits to the diffraction data. They concluded that the root cause of the unusual behavior was in transverse thermal vibrations of bridging O atoms, manifesting in changes in certain Sc–O–W bond angles. We have used a free anisotropic/isotropic model in this case, though we are not suggesting this is the optimum model. We present our resulting M–O–W bond angles in Figs. 7 and 8. A general trend in Evans and colleagues' work was that "large" ($>170°$) angles decrease with temperature, "small" ($<150°$) angles increase with temperature, and "intermediate" angles remain constant. The values for the Sc–O2–W1 angle in the Evans *et al.* paper have been calculated by us from the atomic coordinates supplied, as the plot for this angle was omitted from the original publication. They are shown in Table 3.

The angles involving the W1 ion on the special position exhibit the same trends in $Sc_2(WO_4)_3$, $Al_2(WO_4)_3$, and

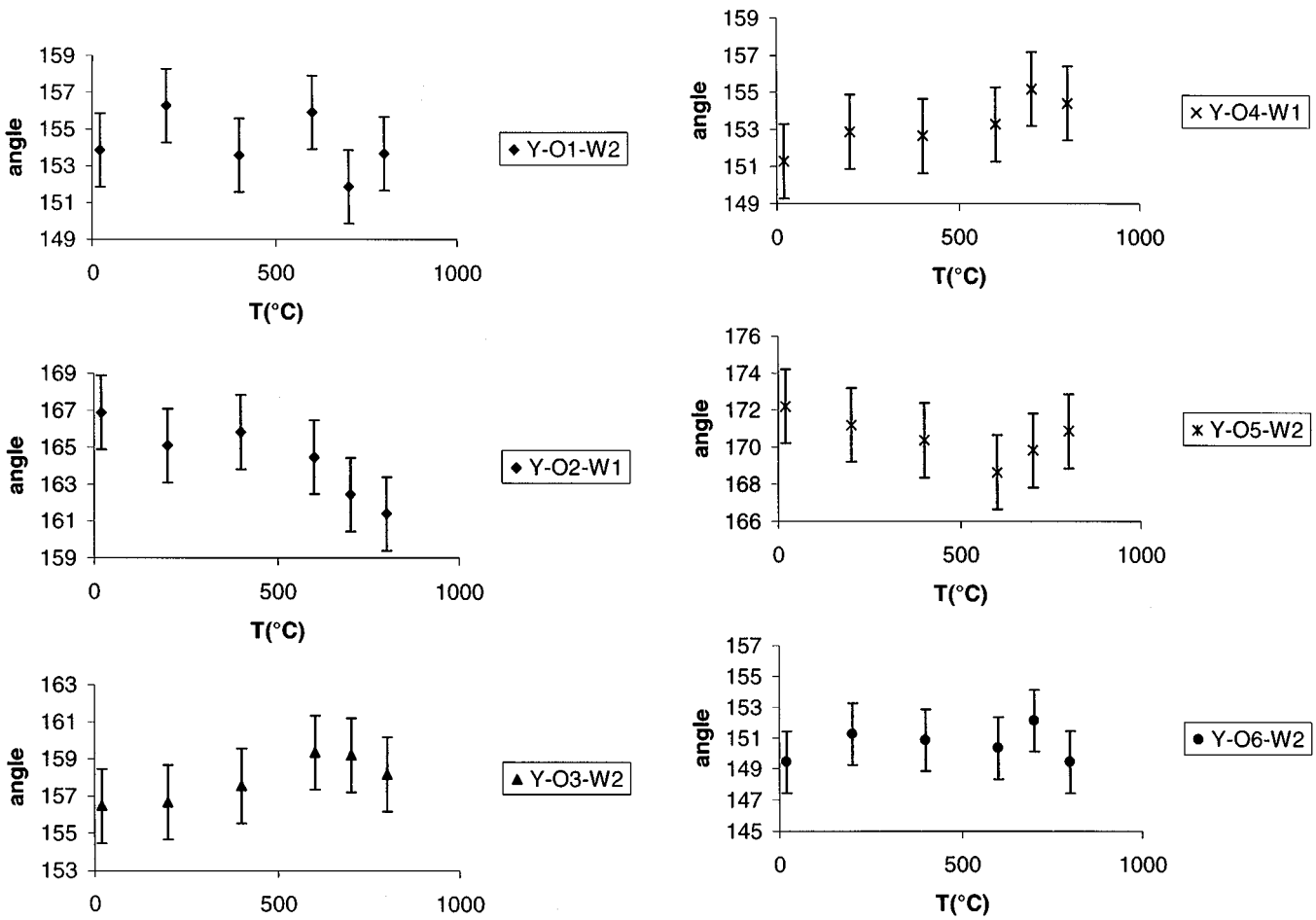

FIG. 7. Thermal evolution of Y–O–W bridging angles.

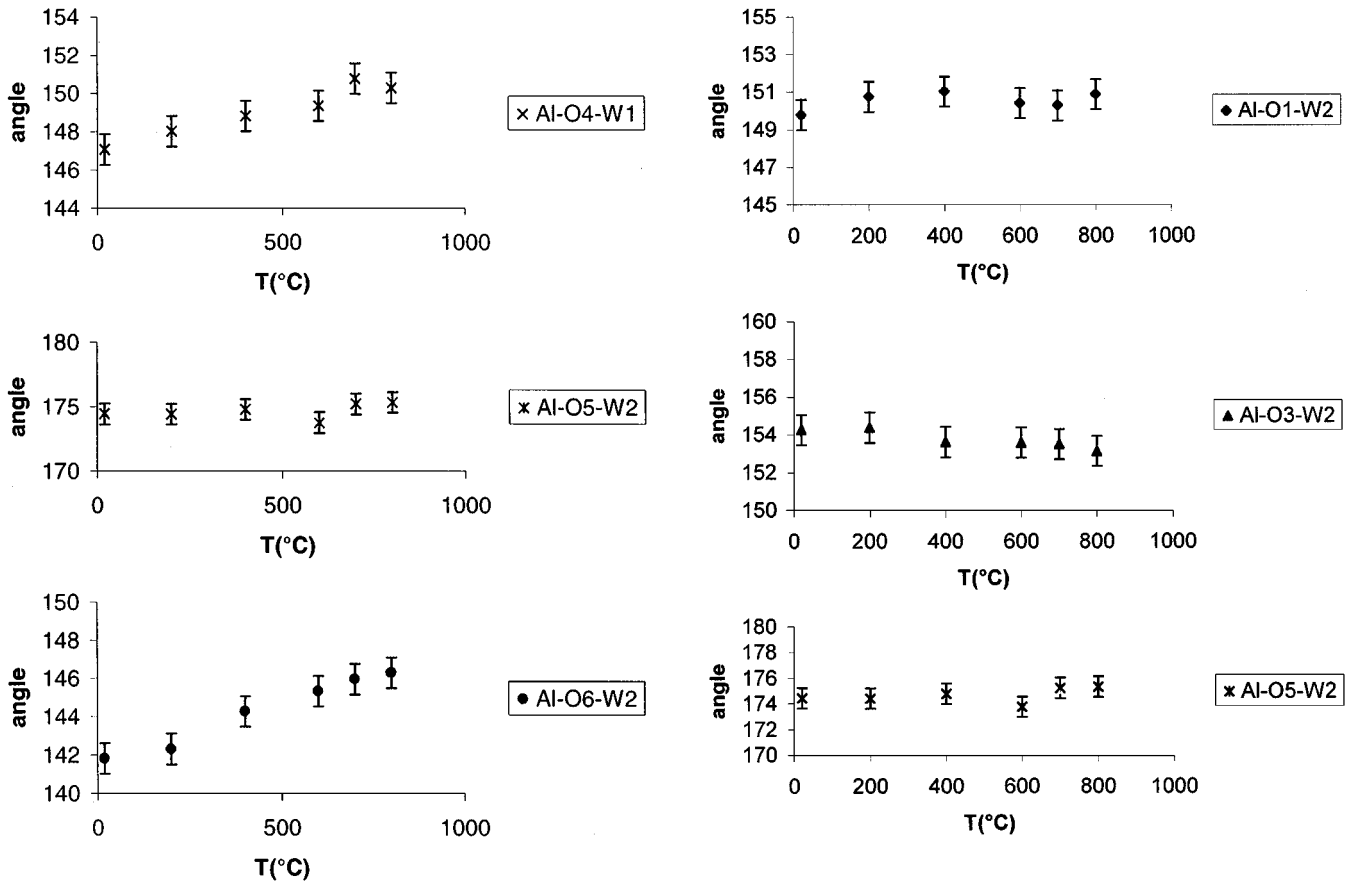

FIG. 8. Thermal evolution of Al–O–W bridging angles.

$Y_2(WO_4)_3$; i.e., *M*–O2–W1 decreases significantly and *M*–O4–W1 increases strongly. $Sc_2(WO_4)_3$ and $Al_2(WO_4)_3$ exhibit the same general thermal expansion properties; i.e., both contract along *a* and *c* and expand along *b* although, in all cases, the effects for Sc are more pronounced.

M–O6–W2 appears to be a key angle, as it remains relatively constant in $Y_2(WO_4)_3$ but increases strongly in both $Sc_2(WO_4)_3$ and $Al_2(WO_4)_3$. This may be related to the fact that the 20°C value of this parameter is significantly larger for $Y_2(WO_4)_3$ than for $Sc_2(WO_4)_3$ and $Al_2(WO_4)_3$. The angles *M*–O1–W2, *M*–O3–W2, and *M*–O5–W2 show little correlation with the different trends in lattice parameters.

TABLE 3
Sc–O–W Bridging Angles

T (K)	Sc–O1–W2	Sc–O2–W1	Sc–O3–W2	Sc–O4–W1	Sc–O5–W2	Sc–O6–W2
10	151.2	173.8	155.1	147.4	175.0	142.6
300	151.7	171.0	154.2	148.3	174.4	144.3
450	151.9	169.7	154.6	149.0	173.4	145.6

CONCLUSIONS

Evans *et al.* (5) suggested that the negative thermal expansivity in the $Sc_2(WO_4)_3$ structure was due to transverse vibrations of the two coordinate bridging oxygen groups, leaving *M*–O bond lengths unchanged but decreasing the average *M*–O–W bridging angle, bringing the two cations closer together. They quantified the tilts of individual bonds and related them to the variations in bridging bond angles. Higher-resolution data would be required to make these calculations and we can only look at general trends involving the *M*–O–W bridging angles. Our results suggest that the *M*–O6–W2 angle shows the greatest difference in thermal behavior between $Al_2(WO_4)_3$, $Sc_2(WO_4)_3$, and $Y_2(WO_4)_3$. The angle is very small for small *M* cations (Al, 142°; Sc, 143°; Y, 150°, at 20°C) and expands significantly on heating. This may be one of the most important parameters influencing the differing behavior of the series.

ACKNOWLEDGMENTS

We thank Peter Cross for help with neutron data collection and the EPSRC for provision of a studentship to D.A.W.

REFERENCES

1. D. A. Woodcock, P. Lightfoot, P. A. Wright, L. A. Villaescusa, M.-J. Díaz-Cabañas, and M. A. Camblor, *J. Mater. Chem.* **9,** 349 (1999).
2. M. P. Attfield and A. W. Sleight, *Chem. Mater.* **10,** 2013 (1998).
3. D. A. Woodcock, P. Lightfoot, and C. Ritter, *Chem. Commun.* 107 (1998).
4. P. Lightfoot, D. A. Woodcock, J. D. Jorgensen, and S. Short, *Int. J. Inorg. Mater.* **1,** 53 (1999).
5. J. S. O. Evans, T. A. Mary, and A. W. Sleight, *J. Solid State Chem.* **137,** 148 (1998).
6. V. A. Balashov, G. I. Vorona, A. A. Maier, and O. P. Proshina, *Inorg. Mater.* **11,** 1469 (1975).
7. P. M. Forster, A. Yokochi, and A. W. Sleight, *J. Solid State Chem.* **140,** 157 (1998).
8. J. S. O. Evans, T. A. Mary, and A. W. Sleight, *J. Solid State Chem.* **133,** 580 (1997).
9. J. Rodriguez-Carvajal, *Physica B* **55,** 192 (1993).
10. S. C. Abrahams and J. L. Bernstein, *J. Chem. Phys.* **45,** 8, 2745 (1966).